Healing of Structural Defects in the Topmost Layer of Graphite by Chemical Vapor Deposition

Iskandar N. Kholmanov, Jonathan Edgeworth, Emanuele Cavaliere, Luca Gavioli, Carl Magnuson, and Rodney S. Ruoff*

Structural defects in graphitic layers have historically received considerable attention, primarily directed towards the behavior of radiation-damaged graphite in nuclear reactors.[1] More recently, efforts have been directed at the crucial role of defects in tailoring the material properties of carbon-based structures such as graphite, carbon nanotubes, and graphene sheets.[2–13] For example, it has been reported that defects are responsible for the inherent ferromagnetic behavior of carbon-based materials, due to the presence around the defects of localized electron states with energies close to that of the Fermi level.[14,15] Very recently, Lahiri et al. reported the controlled production of extended line defects in graphene and suggested that such structures might function as metallic wires.[16] Studies such as these have demonstrated that defect engineering in graphitic systems is a promising approach towards controlling a variety of material properties.

Despite this, defects are well-known for their ability to scatter charge carriers and phonons, thereby decreasing the ballistic transport path length and adversely affecting carrier mobility and thermal conductivity. The detrimental effects of defects are particularly pronounced in graphene films. For example, defects were held responsible for a dramatic reduction in charge carrier mobility in graphene films obtained by micromechanical cleavage.[17] The transport properties of graphene films produced by chemical methods, such as the exfoliation and chemical reduction of graphene oxide platelets, have also been ascribed to defects (introduced by the chemical treatments used).[18] In this respect, defects are undesirable, and the ability to "heal" them is important for generating carbon nanostructures with high electrical and thermal conductivities and, potentially, enhanced mechanical strength. Improvements in these characteristics are of central importance because the successful realization of graphene-based electronic devices requires graphene films with superior transport and structural properties.

One promising approach for removing crystalline lattice defects and restoring graphitic structures is high temperature processing in the presence of a hydrocarbon gas. Using appropriate conditions, the hydrocarbon gas might decompose to supply carbon atoms that can repair defective sites. Recently, López et al. demonstrated that chemical vapor deposition (CVD) processing of chemically derived graphene films using an ethylene carbon source improved film conductivity by two orders of magnitude, to room temperature (RT) values of 10–350 S cm^{-1}.[19] The authors attributed the improvement to defect healing. In addition, direct observation of the modification of defective sites on graphitic surfaces under gaseous hydrocarbon atmospheres was reported by Liu et al., who studied the reactivity of defects on highly oriented pyrolitic graphite (HOPG) surfaces exposed to acetylene at elevated temperatures using scanning tunneling microscopy (STM).[20] In this report, the growth of both amorphous and ordered carbonaceous material at defect sites is directly demonstrated. However, the complete healing of individual defects was not achieved.

In the current work, the healing of artificial defects in the topmost layers of HOPG was studied using STM. Defects with single-layer depth (SLD) and multilayer depth (MLD) were controllably produced by Ar^+ ion beam sputtering with different incidence angles. The depths of the defects were identified using oxidative etching of topmost graphene layers. Defect healing involved a CVD process with iron (Fe) as a catalyst and acetylene (C_2H_2) as the carbon source. It was found that healing depends on the depth of defects and only defects with SLD could be completely healed during this CVD process.

Artificial defects were produced on the (0001) basal plane of freshly cleaved and degassed HOPG surfaces by Ar^+ ion (400 eV) sputtering at room temperature (RT) for 20 s, firstly using a normal incidence angle. **Figure 1**a shows an STM image of an HOPG surface after 20 s of RT sputtering followed by in situ annealing at 900 °C for 10 min. The surface contained sputtering-induced defects with a density (defects per μm^2) of about 7×10^4 μm^{-2}, together with disordered carbon particles a few nanometres in size. The carbon particles are likely formed by the agglomeration of carbon atoms that have been removed from their lattice sites during sputtering. Carbon atom extraction is possible since the energy of the Ar^+ ions (400 eV) is significantly higher than the threshold energy required (≈47 eV).[21] Ar^+ ions with energies this high can eject several carbon atoms from graphene sheets in the HOPG, thereby creating multi-vacancy defects.[22] A representative STM image of a typical individual defect (Figure 1a, inset) shows a hole in the basal plane, formed by the extraction of carbon atoms, surrounded by hillock-like structures.

Dr. I. N. Kholmanov
CNR-IDASC Sensor Lab
Department of Chemistry and Physics
University of Brescia
Via Valotti, 9, Brescia 25133, Italy
E-mail: iskandar.kholmanov@ing.unibs.it
Dr. J. Edgeworth, C. Magnuson , Prof. R. S. Ruoff
Department of Mechanical Engineering and the Texas Materials Institute
University of Texas at Austin
One University Station C2200, Austin, TX 78712, USA
Dr. E. Cavaliere, Dr. L. Gavioli
Department of Mathematics and Physics
Catholic University
via dei Musei 41, Brescia 25121, Italy

DOI: 10.1002/adma.201004019

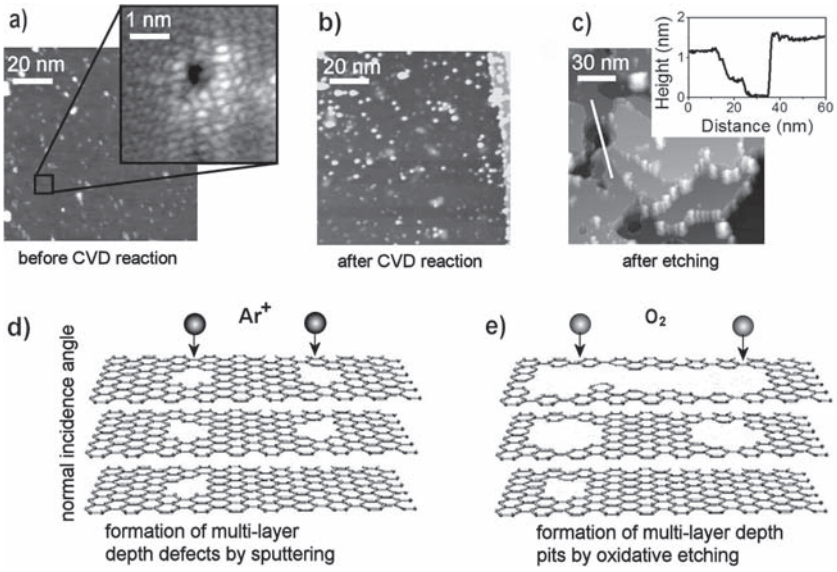

Figure 1. Formation and processing of MLD defects in HOPG surfaces. a) STM image (100 × 100 nm^2, tip–sample bias $V = -1.8$ V, tunneling current $I = 0.1$ nA) of an HOPG surface sputtered using an Ar^+ ion beam with a normal incidence angle and in-situ annealed at 900 °C in an ultrahigh vacuum (UHV) chamber. Inset is an atomically resolved STM image (4 × 4 nm^2, $V = -0.4$ V, $I = 0.2$ nA) showing the detailed morphology of an individual defect. b) STM image (100 × 100 nm^2, $V = -1.4$ V, $I = 0.2$ nA) of the same HOPG surface,after CVD processing, during which no significant morphology changes occurred. c) STM image (150 × 150 nm^2, $V = -2.6$ V, $I = 0.4$ nA) of the sputtered and annealed HOPG after oxidative etching, which results in the formation of MLD pits and extensively etched topmost graphene layers. A constant current profile acquired along the white line is plotted in the inset. d) Schematic illustration of MLD defects produced by Ar^+ ion sputtering with a normal incidence angle. e) Schematic view of MLD pits obtained by oxidative etching of MLD defects. In (d) and (e) Fe nanoparticles are not shown.

Following the generation of defects in HOPG surfaces, 0.1 monolayer (ML) Fe films were deposited onto the samples by electron beam sublimation, as described in the Experimental Section. Deposited Fe preferentially nucleates and agglomerates at the defects in the substrate, by a Volmer–Weber growth mode, to give 3D particles.[23,24] In STM images (not shown), these agglomerate features are not clearly distinguishable from defect structures. With the aim of eliminating the defects through CVD processing, the sample was exposed to pure acetylene gas for 1 min with the sample temperature held at 900 °C. Fe particles, as used here, allow the growth of amorphous carbon to be avoided and may catalyze defect healing during the CVD reaction through their ability to promote the formation of crystalline carbon lattices.[25] However, an STM image of the sample after CVD processing (Figure 1b) indicated no significant decrease in defect density and no change in the overall morphology of the HOPG surface. Identical results were obtained for HOPG surfaces coated in greater amounts of Fe (0.2 ML and 0.3 ML).

These results show that defects produced by the sputtering conditions described above cannot be healed by catalytic CVD processing. A reasonable explanation for this is that the defects in the HOPG sample might have MLDs due to the high energy of the Ar^+ ions used during sputtering.[22] We argue that defects with such depths might be protected from complete healing by the CVD conditions used here. For example, this might be due to an inability of C_2H_2 molecules to penetrate sufficiently far into deep defect structures. Additionally, defects might be stabilized due to the formation of numerous interlayer covalent interactions from the carbon dangling bonds that exist in MLD defects.[6,11]

It is not possible, using STM, to determine the depths of as-produced defects with great certainty due to convolution effects between the sample and the STM tip. Instead, samples were first exposed to an oxidation treatment that partially etched the HOPG graphene layers and "opened" the defects to allow STM analysis of their depths. Figure 1c shows an STM image of an HOPG sample that was sputtered using the conditions described above and decorated with a 0.1 ML Fe film after oxidative etching. The surface shown is extensively etched and characterized by the presence of pits. Large nanoparticles are also visible at the edges of graphene layers; these likely arise from a small proportion of Fe particles that migrate away from defects and then agglomerate at high temperatures.[23] The formation of pits can be rationalized by considering the details of the oxidative etching treatment, described in the Experimental Section. This two-step treatment differed from typical oxidative etching methods, which are often based on the simple annealing of graphite in oxygen-containing atmospheres, by which it is difficult to control the depth of pits formed because of the relatively high oxygen pressures employed.[26,27] In our approach the sample is exposed to oxygen in a more controlled way; the relatively low oxygen pressures applied enabled the avoidance of the random etching of non-defective graphene layers. Etching began at defects in the topmost graphene layer of the HOPG, where oxidized Fe particles were trapped, and progressed in planar directions to form pits. The depths of these pits should depend on the depths of the defects at which they are formed. For MLD defects, illustrated in Figure 1d, etching should result in the formation of pits that are multiple layers deep, as shown in Figure 1e. Therefore, through STM analysis of pit depths, the depths of the original defects could be identified. The pits shown in Figure 1c have MLDs, as shown for an individual pit by the constant current profile in the inset. Thus, sputtering using a 400 eV Ar^+ ion beam with a normal incidence angle results in the production of MLD defects.

To produce HOPG surfaces containing SLD defects, clean HOPG surfaces were sputtered with Ar^+ ion beams with an increased incidence angle. **Figure 2**a shows an STM image of an HOPG surface sputtered using a 75° incidence angle. The surface is characterized by an average defect density of 2.0 × 10^4 μm^{-2}. An atomically resolved STM image of an individual defect (Figure 2a, inset) shows a morphology that is distinguishable from that of the MLD defects (e.g., Figure 1b). Such morphologies can be ascribed to surface vacancy defects surrounded by strong crystalline lattice distortions in the regular honeycomb structure.[28] Similar features have been observed in STM images of bilayer graphene sheets grown on SiC surfaces.[29]

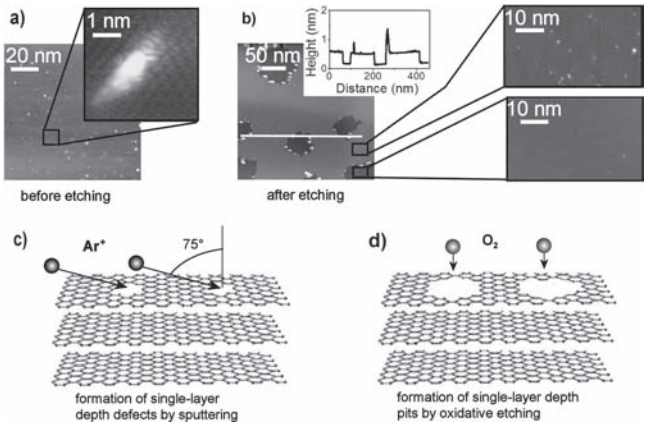

Figure 2. Formation and oxidative etching of SLD defects in HOPG surfaces. a) STM image (100 × 100 nm^2, V = –1 V, I = 0.25 nA) of an HOPG surface after sputtering using an Ar^+ ion beam with 75° incidence angle and in situ annealing at 900 °C in an UHV chamber. Atomically resolved STM image (4 × 4 nm^2, V = –0.1 V, I = 0.1 nA) of an individual defect is shown in the inset. b) STM image (280 × 280 nm^2, V = –1.4 V, I = 0.14 nA) of the same HOPG surface after oxidative etching, showing only SLD pits, as indicated by the inset constant current profile, which correspond to the white line in the main image. Comparison of higher magnification STM images of the topmost (upper image 50 × 30 nm^2, V = –1 V, I = 0.25 nA) and first exposed (lower image 50 × 30 nm^2, V = –1 V, I = 0.25 nA) graphene layers demonstrates that the defects have SLD. c) Schematic illustration of SLD defects produced by Ar^+ ion sputtering with 75° incidence angle. d) Schematic view of SLD pits obtained by oxidative etching of SLD defects. In (c) and (d) Fe nanoparticles are not shown.

The depths of defects produced using a 75° incidence angle were verified in the same way as those produced using a normal incidence angle. Figure 2b shows an STM image of a sample that was sputtered using a 75° incidence angle and decorated with Fe after oxidative treatment. Oxidative etching occurred exclusively in the topmost graphene layer, creating pits of SLD, as indicated by the constant current profile shown in the inset of Figure 2b. Layers beneath the topmost sheet were not damaged during the etching process and remained almost defect-free. SLD pits should form from defects with SLDs, as described above and illustrated in Figures 2c,d. These observations indicate that Ar^+ ion sputtering with an incidence angle of 75° results in the formation of SLD defects on the topmost graphene layer of HOPG.

To test whether SLD defects could be healed by CVD processing, HOPG samples with SLD defects decorated by Fe nanoparticles were exposed to acetylene under CVD conditions identical to those used for MLD defects. STM images of the sample before and after CVD treatment are shown in **Figure 3**a,b, respectively. In contrast to HOPG surfaces with MLD defects (Figure 1b), for this sample a significant change in surface morphology was observed after CVD processing. Most of the defects in the topmost graphene layer were completely healed, resulting in a dramatic reduction in the defect concentration from 2.0 × 10^4 μm^{-2} to about 0.5 × 10^2 μm^{-2} and resulting in the restoration of the graphene lattice to a perfect honeycomb structure. Complete elimination of individual SLD defects in topmost graphene layers might be possible since they are entirely open to exposure to hydrocarbon molecules during the CVD process. Moreover, the topmost defective layer lies on an underlying defect-free graphene sheet that is flat and chemically inert. In this case, carbon atoms at defect sites can have no out-of-plane interactions with those in deeper layers, so defect reparation cannot be hindered by interplanar chemical interactions.

It should be noted that prior to carrying out the work described above, preliminary control experiments were conducted to verify the role of Fe during oxidative etching and CVD processing. For sputtered and annealed HOPG samples, STM analysis revealed that oxidative treatment without Fe lead to less effective etching and little correlation between the sputtering incidence angle and pit depth. The presence of Fe was also found to be important in CVD processing: for HOPG samples with SLD defects that were not decorated with Fe, CVD processing resulted in no defect healing and small amounts of amorphous carbon at step edges. Thus, we suggest that Fe acts as a catalyst during high-temperature CVD processing. This was also predicted very recently for nickel-graphene systems.[30]

We suggest that this approach will work for healing SLD defects in bilayer and few-layer graphene sheets where the topmost graphene layer or sheets can behave similarly to that of HOPG. In addition, one can expect that it may work for suspended single-layer graphene sheets. However, for single-layer substrate-supported graphene sheets the healing of SLD defects may depend on the nature of the interaction of carbon atoms at defect sites with the substrate. Strong out-of-plane chemical interactions in these locations, which might be further promoted by local substrate characteristics such as roughness, terraces, and various types of defects, could prevent defect healing.

In summary, structural defects were produced on HOPG surfaces by Ar^+ ion sputtering and their healing by CVD using acetylene as a carbon feedstock gas was studied. The depths of the defects were controlled using the sputtering incidence angle and were identified through oxidative etching of the HOPG surfaces and STM examination of the pits thereby formed. It was found

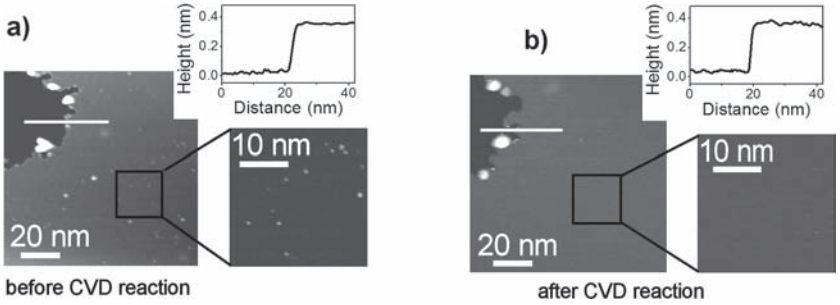

Figure 3. Healing of SLD defects in HOPG surfaces by CVD processing. STM images (100 × 100 nm^2) of an HOPG surface with SLD defects a) before (V = –1.4 V, I = 0.14 nA) and b) after (V = –1.8 V, I = 0.12 nA) CVD processing. The inset STM images (40 × 40 nm^2) in (a) and (b) demonstrate the presence and elimination of defects prior to and after the CVD reaction, respectively. Constant current profiles (acquired along the white lines shown in the corresponding main images) show SLD pits produced by oxidative etching of the topmost graphene layer.

that only SLD defects could be healed during the CVD reaction and that the presence of Fe particles that were deposited onto the defective film was crucial to avoid formation of amorphous carbon. The methods described in this work hold significant promise for healing defective surfaces of graphite, graphene, and graphene-based materials, and hence for improving their structural, electrical, and mechanical properties. Such improvements are vital for the successful realization of graphene-based electronic devices.

Experimental Section

All experiments were performed inside an Omicron STM/SEM/SAM (scanning tunnelling microscopy/scanning electron microscopy/scanning Auger microscopy) UHV system with a base pressure below 5×10^{-11} mbar. This system consisted of three chambers connected in series: 1) entry lock (EL), 2) sample preparation, and 3) analysis. A detailed description of the experimental setup was provided elsewhere.[25,31] HOPG (ZYB grade, Micromasch) was cleaved in air and immediately inserted into the experimental chamber, where it was thoroughly degassed at 900 °C until the chamber pressure fell below 5×10^{-10} mbar. Sample cleanliness was checked in the analysis chamber using STM and Auger spectroscopy.

Artificial defects were produced on HOPG surfaces by sputtering with an Ar^+ ion beam (400 eV) in the sample preparation chamber, using one of two different incidence angles (normal and 75°), at a pressure of 2.7×10^{-7} mbar. In all cases, sputtering was immediately followed by sample annealing at 900 °C.

Fe films were deposited by electron beam sublimation with the HOPG substrates at RT. The nominal Fe deposition rate was measured using a quartz oscillator. One ML of Fe was defined here as the surface density of the bcc metal, i.e., 12.17×10^{14} atoms per cm^2.

Oxidative etching involved a two-step process: 1) Fe decorated defective HOPG surfaces at RT were exposed to pure oxygen gas for 1 min, which increased the pressure inside the EL chamber (base pressure 5×10^{-7} mbar) to 5×10^{-1} mbar and 2) the samples were subsequently annealed at 800 °C for 5 min in the sample preparation chamber under a flow of O_2 gas that caused the chamber pressure to increase from 5×10^{-10} mbar to 1.5×10^{-7} mbar.

The CVD process was performed in the sample preparation chamber. The temperature of the HOPG samples was first raised from RT to 900 °C by direct current heating, which required approximately 1 min. Once at 900 °C, the HOPG was exposed to acetylene gas; the chamber pressure during this step was 7.5×10^{-7} mbar. After 1 min exposure, the heating power was switched off and the sample was cooled for 2 min. Samples were transferred to the analysis chamber (pressure $< 5 \times 10^{-11}$ mbar) for STM studies.

The STM images presented in this work were obtained in constant current mode at RT using tungsten tips.

We note that defect healing has been investigated in HOPG samples with different defect densities. Different defect densities were obtained by varying several parameters of Ar^+ ion beam sputtering, such as incidence angle, dose, and beam energy. Additionally, CVD processing using different conditions (temperature T = 800–1100 °C, pressure $P = 5.0 \times 10^{-8}$–1.0×10^{-5} mbar, time t = 0.5–4 min) was carried out to find optimal conditions for defect healing. The CVD conditions described in this work enabled highly efficient healing of SLD defects, with the occurrence of healing independent of defect density. No healing of MLD defects was observed using any set of experimental conditions.

Acknowledgements

I.N.K. thanks the CNR Short-Term Mobility Program and the University of Texas (UT) at Austin for his stay at UT. R.S.R. thanks the Semiconductor Research Corporation and C.M. thanks the DOE for fellowship support. J.E. appreciates support from the Institute of Advanced Technology at UT-Austin.

Received: October 31, 2010
Revised: January 15, 2010
Published online: February 15, 2011

[1] J. H.W. Simmons, *Radiation Damage in Graphite*, Pergamon Press, Oxford, UK **1965**.
[2] E. V. Castro, M. P. López-Sancho, M. A. H. Vozmediano, *Phys. Rev. Lett.* **2010**, *104*, 036802.
[3] J. Červenka, M. I. Katsnelson, C. F. J. Flipse, *Nat. Phys.* **2009**, *5*, 840.
[4] D. A. Dikin, S. Stankovich, E. J. Zimney, R. D. Piner, G. H. B. Dommett, G. Evmenenko, S. T. Nguyen, R. S. Ruoff, *Nature* **2007**, *448*, 457.
[5] D. W. Boukhvalov, M. I. Katsnelson, *Nano Lett.* **2008**, *8*, 4373.
[6] V. Krasheninnikov, F. Banhart, *Nat. Mater.* **2007**, *6*, 723.
[7] A. Hashimoto, K. Suenaga, A. Gloter, K. Urita, S. Iijima, *Nature* **2004**, *430*, 870.
[8] C. Gómez-Navarro, P. J. De Pablo, J. Gómez-Herrero, B. Biel, F. J. Garcia-Vidal, A. Rubio, F. Flores, *Nat. Mater.* **2005**, *4*, 534.
[9] M. T. Lusk, L. D. Carr, *Phys. Rev. Lett.* **2008**, *100*, 175503.
[10] A. H. Castro Neto, F. Guinea, N. M. R. Peres, K. S. Novoselov, A. K. Geim, *Rev. Mod. Phys.* **2009**, *81*, 109.
[11] R. H. Telling, Ch. P. Ewels, A. A. El-Barbary, M. I. Heggie, *Nat. Mater.* **2003**, *2*, 333.
[12] J. H. Warner, M. H. Rümmeli, L. Ge, T. Gemming, B. Montanari, N. M. Harrison, B. Büchner, G. A. D. Briggs, *Nat. Nanotechnol.* **2009**, *4*, 500.
[13] J. C. Meyer, C. Kisielowski, R. Erni, M. D. Rossell, M. F. Crommie, A. Zettl, *Nano Lett.* **2008**, *8*, 3582.
[14] M. M. Ugeda, I. Brihuega, F. Guinea, J. M. Gómez-Rodríguez, *Phys. Rev. Lett.* **2010**, *104*, 096804.
[15] H. Ohldag, T. Tyliszczak, R. Höhne, D. Spemann, P. Esquinazi, M. Ungureanu, T. Butz, *Phys. Rev. Lett.* **2007**, *98*, 187204.
[16] J. Lahiri, Y. Lin, P. Bozkurt, I. I. Oleynik, M. Batzill, *Nat. Nanotechnol.* **2010**, *5*, 326.
[17] K. Kim, H. J. Park, B.-C. Woo, K. J. Kim, G. T. Kim, W. S. Yun, *Nano Lett.* **2008**, *8*, 3092.
[18] A. B. Kaiser, C. Gómez-Navarro, R. S. Sundaram, M. Burghard, K. Kern, *Nano Lett.* **2009**, *9*, 1787.
[19] V. López, R. S. Sundaram, C. Gómez-Navarro, D. Olea, M. Burghard, J. Gómez-Herrero, F. Zamora, K. Kern, *Adv. Mater.* **2009**, *21*, 4683.
[20] L. Liu, K. T. Rim, D. Eom, T. F. Heinz, G. W. Flynn, *Nano Lett.* **2008**, *8*, 1872.
[21] D. Marton, K. J. Boyd, T. Lytle, J. W. Rabalais, *Phys. Rev. B* **1993**, *48*, 6757.
[22] J. R. Hahn, H. Kang, *Surf. Sci.* **2000**, *446*, L77.
[23] I. N. Kholmanov, L. Gavioli, M. Fanetti, M. Casella, C. Cepek, C. Mattevi, M. Sancrotti, *Surf. Sci.* **2007**, *601*, 188.
[24] C. Binns, S. H. Baker, C. Demangeat, J. C. Parlebas, *Surf. Sci. Rep.* **1999**, *34*, 107.
[25] I. N. Kholmanov, M. Cavalieire, C. Cepek, L. Gavioli, *Carbon* **2010**, *48*, 1619.
[26] L. Liu, R. Sunmin, M. R. Tomasik, E. Stolyarova, N. Jung, M. S. Hybertsen, M. L. Steigerwald, L. E. Brus, G. W. Flynn, *Nano Lett.* **2008**, *8*, 1965.
[27] F. Stevens, L. A. Kolodny, T. P. Jr. Beebe, *J. Phys. Chem. B* **1998**, *102*, 10799.
[28] P. Ruffieux, M. Melle-Franco, O. Gröning, M. Bielmann, F. Zerbetto, P. Gröning, *Phys. Rev. B* **2005**, *71*, 153403.
[29] G. M. Rutter, J. N. Crain, N. P. Guisinger, T. Li, P. N. First, J. A. Stroscio, *Science* **2007**, *317*, 219.
[30] S. Karoui, H. Amara, C. Bichara, F. Ducastelle, *ACS Nano* **2010**, *4*, 6114.
[31] I. N. Kholmanov, E. Cavalieire, M. Fanetti, C. Cepek, L. Gavioli, *Phys. Rev. B.* **2009**, *79*, 233403.